Dual Nature of a Ni Dopant in the Hole-Type $La_{2-x}Sr_xCuO_4$ Cuprate Superconductor

H. Hiraka,[1] D. Matsumura,[2] Y. Nishihata,[2] J. Mizuki,[2] and K. Yamada[3]

[1]*Institute for Materials Research, Tohoku University, Sendai 980-8577, Japan*

[2]*Quantum Beam Science Directorate, Japan Atomic Energy Agency, Hyogo 679-5148, Japan*

[3]*Advanced Institute for Materials Research (WPI), Tohoku University, Sendai 980-8577, Japan*

(Received 2 March 2008; published 21 January 2009)

Local distortions around a Ni dopant in the hole-type $La_{2-x}Sr_xCuO_4$ superconductor system were studied by x-ray-absorption fine structure (XAFS) using single crystals over a wide hole-doping range. Two distinct interatomic distances between Ni and in-plane oxygen appear in the Ni *K*-edge extended XAFS. Combined with previous results on hole-localization effects by Ni doping, two types of charge states are strongly indicated for Ni. This duality disqualifies a magnetic-impurity picture for Ni dopant in the superconducting phase of cuprates.

DOI: 10.1103/PhysRevLett.102.037002 PACS numbers: 74.62.Dh, 61.05.cj, 74.72.Dn

In conventional *s*-wave superconductors, localized spin impurity breaks down Cooper pairs and damages superconductivity substantially [1]. Nonmagnetic impurity also degrades the superconductivity by changing the number of free electrons and the density of states, for example. In that case, however, the reduction rate in T_c is more moderate than that by magnetic impurity, since no magnetic scattering arises. On the contrary, impact on high T_c from nonmagnetic impurity appears quite large in cuprate *d*-wave superconductors [2], which is still an issue remaining to be resolved. According to past intensive studies for spinless impurity of Zn, the spin-half network on the CuO_2 plane is severely destroyed by Zn, and its superconducting (SC) state is locally broken down around Zn [3]. Therefore, a spin-1/2 network should be essential to sustain superconductivity in high-T_c cuprates. To confirm this conjecture, it is required to investigate doping effects of impurity which does not disturb the spin-1/2 network. Ni dopant is one candidate for such an impurity because a possible ''hole-absorber'' feature giving $S = 1/2$ with Ni^{3+} has been indirectly argued in a macroscopic phase diagram [4], bulk magnetic susceptibility [5,6], and magnetic neutron scattering [7–9]. Here, we site-selectively inspect such a hole-absorber feature of Ni dopant by means of x-ray-absorption-fine-structure (XAFS) measurements.

XAFS spectroscopy is a good tool for such research because of the element selectivity and good sensitivity for the valence state and the local structure. Haskel *et al.* [10] measured XAFS of Ni-doped $La_{2-x}Sr_xCuO_4$ (LSCO) of $x = 0.15$ using magnetically oriented powder samples. By quantitative data analyses for the extended XAFS (EXAFS) spectra, they found that the local distance of Ni-O(2) (apical oxygen) is very close to that of La_2NiO_4, while the local distance of Ni-O(1) (in-plane oxygen) equals that of surrounding Cu-O(1). They indicated that a $3d^8$ (Ni^{2+}) electronic configuration with $S = 1$ causes the local *c*-axis contraction by the non-Jahn-Teller nature. Although doped holes were supposed to distribute over O(1) sites and localize around Ni, they paid little attention to the role of O(1), and their study was limited to only optimally hole-doped samples.

In this Letter, we present fluorescence Ni *K*-edge XAFS spectra for Ni-doped LSCO single crystals over a wide hole-doping range. Distinct two types of Ni-O(1) bond length appear in the raw XAFS and, surprisingly, they depend on a simple balance between the hole and Ni contents. We speculate that this novel local structure arises from a dual charge state of the Ni dopant by trapping a hole. Present XAFS study succeeds in bridging consistently the magnetic-impurity state $S = 1$ and the charge-impurity state $Ni^{2+}\underline{L}$ of Ni dopant, where $\underline{L}$ represents a ligand hole bound on O(1). As a result, past arguments for magnetic-impurity effects on high-T_c superconductivity should be reconsidered.

Polarized XAFS experiments were performed on the beam line BL14B1 at SPring-8, Japan. An energy resolution of approximately ~1 eV was achieved by using a Si(111) double-crystal monochromator. Ni *K*-edge XAFS spectra were measured using single crystals (typical size $\sim 5 \times 5 \times 3$ mm^3) at room temperature. A multi solid-state-detector bank of Ge was applied to monitor fluorescence spectra. Two types of geometries of $\mathbf{E} \parallel CuO_2$ plane ($\mathbf{E}_\parallel$) and $\mathbf{E} \perp CuO_2$ plane ($\mathbf{E}_\perp$) were used, where $\mathbf{E}$ represents an electrical-field vector of the incident x-ray (inset of Fig. 1). In some cases, the azimuthal angle or the crystal angle was rotated by $\leq 10°$ as an offset to eliminate contamination from Bragg diffraction. Ni-doped single crystals of $La_{2-x}Sr_xCu_{1-y}Ni_yO_4$ of $0 \leq x \leq 0.15$ and $0.01 \leq y \leq 0.07$ were grown by traveling-solvent-floating-zone techniques and subsequently annealed under either O_2 or Ar flowing gas. Hereafter, we specify the concentrations of hole and Ni as $(100x - 100y)$ for each sample. Also, a single crystal of nickelate $La_{1.95}Sr_{0.05}NiO_4$ was prepared for the reference of Ni^{2+} state [11]. The magnetic properties of these single crystals have been described elsewhere [7,9,12]. Further, the stoichiometry

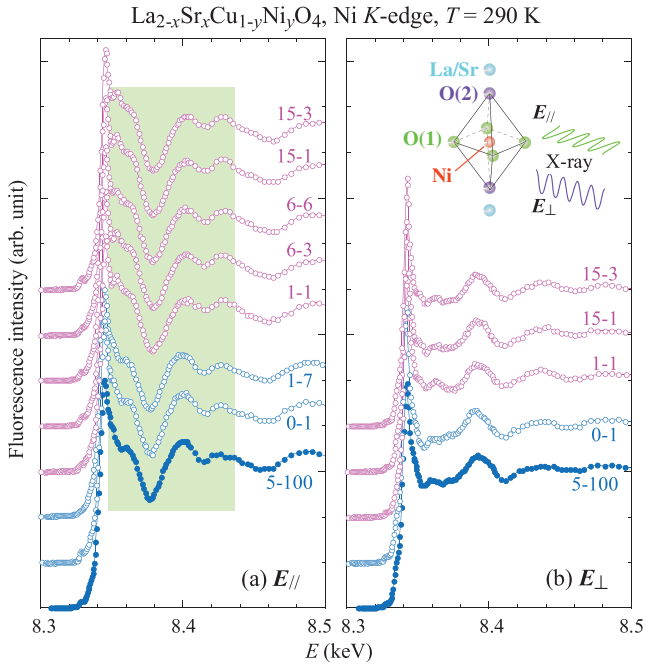

FIG. 1 (color). Raw data of polarized XAFS at Ni K-edge using single crystals of $La_{2-x}Sr_xCu_{1-y}Ni_yO_4$ for (a) $\mathbf{E}_\parallel$ and (b) $\mathbf{E}_\perp$. The Ni^{2+} standard sample of (5–100) is included. Here, the hole and Ni concentrations are expressed as $(100x - 100y)$.

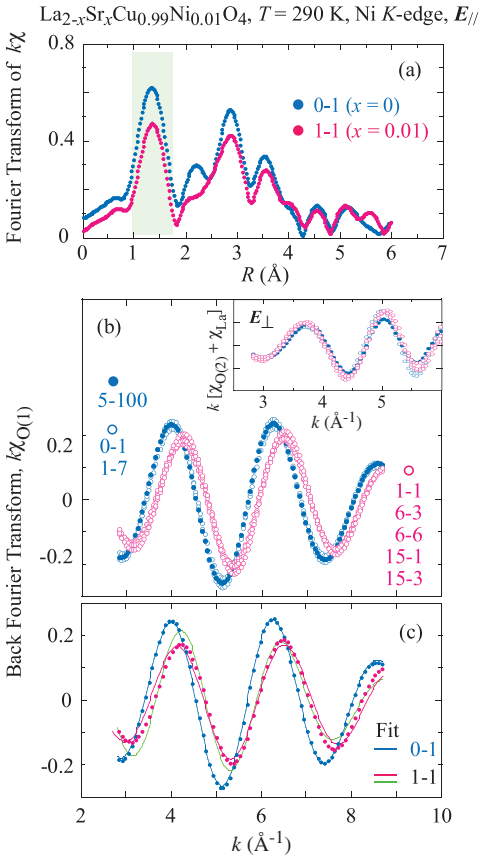

FIG. 2 (color). (a) Fourier transforms of $k\chi$ for two representative samples (0-1) and (1-1) when $\mathbf{E}_\parallel$. (b) In-plane O(1) component, $k\chi_{O(1)}$, from all samples after back-Fourier transforms. For comparison, the out-of-plane component of $k[\chi_{O(2)} + \chi_{La}]$ from $\mathbf{E}_\perp$ setup is shown in the inset. (c) Fits to $k\chi_{O(1)}$ by using the typical data set of (0-1, blue dots) and (1-1, red dots). Regarding the detailed fitting approach, see the text.

of some crystals was chemically checked by ICP spectroscopy.

Figures 1(a) and 1(b) show raw data of polarized Ni K-edge XAFS in the relatively low photon-energy side with the geometries of $\mathbf{E}_\parallel$ and $\mathbf{E}_\perp$, respectively. In the green-hatch region of Fig. 1(a), an apparent difference appears in the intensity pattern between the upper five and the lower three spectra for $\mathbf{E}_\parallel$. Unexpectedly, the former red-colored group has a concentration of $x \geq y$ (hole rich), whereas the latter blue-colored one exhibits the opposite concentration of $x < y$ (Ni rich). Since the Ni-rich group contains the Ni^{2+} reference, the charge state of Ni dopant is regarded as Ni^{2+} in average [13]. On the contrary, a higher valence state than Ni^{2+} or a strongly hole-bound state around Ni is expected to occur in the hole-rich group because a positive edge-energy shift by $\sim$1 eV appears as compared with the Ni-rich group [14]. In contrast, the concentration dependence for $\mathbf{E}_\perp$ is less pronounced, as shown in Fig. 1(b). This distinct polarization dependence confirms that bound holes by Ni are well confined on the CuO_2 plane. Therefore, the in-plane O(1) rather than the apical O(2) will be a clue to clarify the hole-bound state. Concerning the weak pre-edge intensity at $\sim$8.33 keV, further systematic investigation is required with high statistics.

The influence of such a hole-bound state on the CuO_2 plane is visible on the local distortion of the $NiO(1)_4$ square for $\mathbf{E}_\parallel$. Figure 2(a) shows examples of Fourier transforms of $k\chi(k)$ as a function of the distance from Ni, R, where $\chi(k)$ is the EXAFS function obtained from high-energy oscillations. Note that the difference of the two typical samples with (0-1) and (1-1) is only the hole concentration by 1%. The k range used in the Fourier transform is $2.5 \leq k \leq 9$ Å^{-1}. The first peak at $R \sim 1.4$ Å is caused by the nearest-neighbor O(1), in which we are interested. Using back-Fourier filter around the O(1) peak [green hatch in Fig. 2(a)], the O(1) component $k\chi_{O(1)}(k)$ was picked up. Figure 2(b) shows such $k\chi_{O(1)}$ for all samples. The data distribute fairly into two series: one is the hole-rich group and the other the Ni-rich one. The different periodicity in k space is apparent, which corresponds in real space to the shorter Ni-O(1) length for the hole-rich group than that for the Ni-rich group. The second remark is the small amplitude among the hole-rich group, indicating a substantial contribution of hole for the weakened interference between photoelectrons. In contrast, the out-of-plane component from O(2) plus La, $k[\chi_{O(2)} + \chi_{La}]$, shows no difference in the periodicity as well as the amplitude between the hole-rich and Ni-rich groups, as

seen in the inset of Fig. 2(b) [15]. It strongly suggests that the interatomic distance of Ni-O(2) is independent of x and y. It should be noteworthy that these qualitative natures are all derived without using any theoretical model.

To evaluate the hole binding effect on the in-plane Ni-O(1) bond quantitatively, we use EXAFS formulae [16] of $\chi(k) = \sum_{i\,\mathrm{shell}} \chi_i(k)$ with

$$\chi_i(k) = C_i F_i(k) \exp(-2\sigma_i^2 k^2) \frac{\sin[2kR_i + \Phi_i(k)]}{kR_i^2}, \quad (1)$$

where $F_i(k)$, σ_i^2, $\Phi_i(k)$, and R_i represent the backscattering factor, Debye-Waller factor, phase shift, and distance between Ni and the surrounding atom in the i shell, respectively. C_i is a product of the coordination number and the intrinsic loss factor. Below, we focus on the O(1) shell at first, in particular, on $R_{O(1)}$. Preliminary to the next curve fitting, we determined $C_{O(1)}$, $F_{O(1)}(k)$, $\sigma^2_{O(1)}$, and $\Phi_{O(1)}(k)$ using the Ni^{2+} reference under the condition of $R_{O(1)} = 1.94$ Å [17].

The blue line in Fig. 2(c) is a fit to the (0-1) data using $R_{O(1)}$ as a free parameter with fixed $C_{O(1)}$, $F_{O(1)}(k)$, $\sigma^2_{O(1)}$, and $\Phi_{O(1)}(k)$ from the Ni^{2+} reference. The agreement between the data and fit is excellent, and the obtained $R_{O(1)}$ and the fixed $C_{O(1)}$ are plotted at $x_{\mathrm{eff}} \equiv x - y = -1$ in Fig. 3. On the other hand, the green line in Fig. 2(c) is a conventional fit to the (1-1) data using $R_{O(1)}$ and $\sigma^2_{O(1)}$ as free parameters with fixed $C_{O(1)}$, $F_{O(1)}(k)$, and $\Phi_{O(1)}(k)$ from the Ni^{2+} reference. The discrepancy of peak height is large particularly below $k \sim 4$ Å^{-1}. The red line improves the fit, in which $R_{O(1)}$ and $C_{O(1)}$ are used as free parameters and $F_{O(1)}(k)$, $\sigma^2_{O(1)}$, and $\Phi_{O(1)}(k)$ from the Ni^{2+} reference are fixed. Such $R_{O(1)}$ and $C_{O(1)}$ for the other samples are plotted in Fig. 3. $R_{O(1)}$ equals the distance of Ni-O(1) of La_2NiO_4 [17] for $x_{\mathrm{eff}} < 0$, and that of Cu-O(1) of La_2CuO_4 [18] for $x_{\mathrm{eff}} \geq 0$. Note that the discontinuity in $R_{O(1)}$ by ~0.05 Å is irrelevant to the bulk structural phase transition at $x \simeq 0.10$ [19]. $C_{O(1)}$ in the hole-rich group decreases by ~25% as compared with that determined from the Ni^{2+} reference.

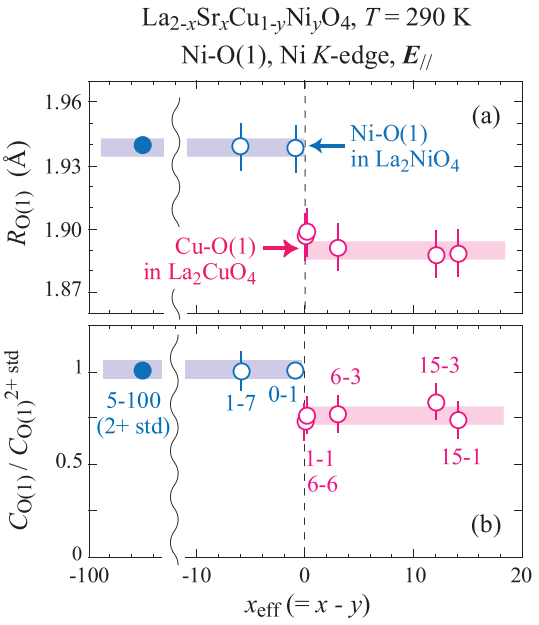

FIG. 3 (color). (a) The bond length $R_{O(1)}$ and (b) the normalized $C_{O(1)}$ as a function of x_{eff}. The blue and red arrows in (a) correspond to the Ni-O(1) distance in La_2NiO_4 [17] and the Cu-O(1) distance in La_2CuO_4 [18], respectively.

We briefly mention the out-of-plane component, which was evaluated from a two-shell analysis [15]. $R_{O(2)}$ becomes nearly equal to that in La_2NiO_4 and it is considerably shorter than the distance of Cu-O(2) in La_2CuO_4, as previously noted [10]. However, in contrast to the O(1) component, both $R_{O(2)}$ and $C_{O(2)}$ are completely insensitive to x_{eff}, as expected from the inset of Fig. 2(b). These facts strongly support the in-plane confinement of trapped holes.

The highlight of current XAFS experiments is the distinct two Ni-dopant states that are clearly visible in the raw data for $\mathbf{E}_{\parallel}$ [Figs. 1(a) and 2(b)]. Since the early XAFS measurement by Haskel *et al.* was limited to samples of $x_{\mathrm{eff}} > 0$ [10], only the hole-bound state was investigated and no change was found in $R_{O(1)}$. Also, our conclusion is quite different from the consequence based on indirect measurements of magnetic susceptibility [6], in which a Ni^{3+} state with a free spin of $S = 1/2$ was supposed to arise in the overdoped phase. First, the strongly hole-bound state should be represented by $Ni^{2+}\underline{L}$ rather than Ni^{3+}, because of the charge-transfer Mott insulator. In fact, the edge-energy shift for the $Ni^{2+}\underline{L}$ state [14] is about half of that for Ni^{3+} in $LaNiO_3$ (~2 eV) [20]. Second, the Ni spin should be correlated strongly with surrounding Cu spins. Third, the $Ni^{2+}\underline{L}$ state is realized even in the lightly hole-doped antiferromagnetic phase.

Figure 4 schematically shows our results from the charge, lattice, and spin viewpoints. First, two types of ligand holes are present on O(1): mobile one around Cu

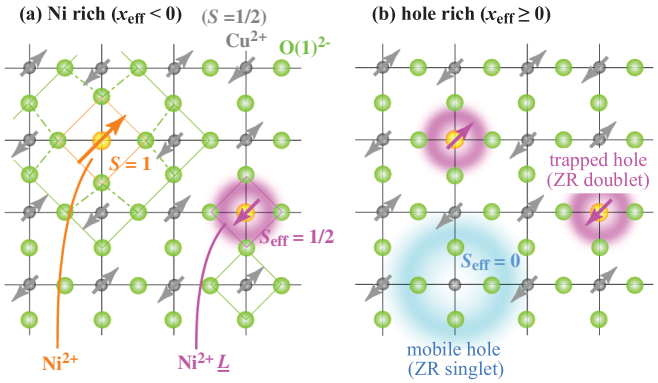

FIG. 4 (color). Schematics of the Ni-doped CuO_2 plane in the (a) Ni-rich and (b) hole-rich groups. The red (blue) clouds around Ni (Cu) represent spatially trapped (mobile) holes.

and localized one around Ni. The former is loosely bound around Cu, resulting in a spin-singlet Zhang-Rice (ZR) state [21]. Next, the in-plane local structure settles down to that of either La_2CuO_4 or La_2NiO_4. Note that the dimension of $NiO(1)_4$ square matches the CuO_2 plane by trapping a hole. Therefore, the replacement with Ni may give weak effect on the local structure in the hole-rich group, especially. Last, two types of Ni spin state are expected: $S_{\rm eff} = 1/2$ for $Ni^{2+}\underline{L}$, and $S = 1$ for Ni^{2+}. The former corresponds to a well-localized ZR doublet state, in which a hole spin on O(1) is strongly bound around Ni and antiferromagnetically couples with the localized Ni spin. As a result, a Ni atom can function as either a hole absorber without giving impact on spin-1/2 magnetic framework (i.e., charge dopant), or a magnetic impurity without disturbing divalent charge framework (i.e., magnetic dopant).

This dual picture for Ni dopant can coherently explain the Ni-doping dependence of spin structure as well as the Néel temperature (T_N) in the lightly hole-doped antiferromagnet $La_{1.99}Sr_{0.01}Cu_{1-y}Ni_yO_4$ with $0 \le y \le 0.10$ [7]. Namely, the charge-dopant feature reduces $x_{\rm eff}$ and explains the substantial increase of T_N for the dilute Ni doping ($y \le 0.02$), whereas the drastic spin rotation at $y \simeq 0.05$ from the La_2CuO_4 type ($\mathbf{S} \parallel \mathbf{b}$) to the La_2NiO_4 type ($\mathbf{S} \parallel \mathbf{a}$) is attributed to the magnetic-dopant nature (or, the single-ion anisotropy of $S = 1$).

Let us inspect the past data on Ni-doping effects for the SC phase of cuprates, where $x_{\rm eff} \ge 0$. The minimum perturbation by the ZR doublet state on the underlying spin and lattice frameworks can explain the tiny paramagnetic moment of Ni dopant [22], and the weak degrade of T_c [2] and the SC coherence peaks [23], as compared with Zn-doping effects [3]. Moreover, the context of $x_{\rm eff}$ (i.e., the Ni-induced underdoping) well explains the following: the reduction of the magnetic neutron-resonance energy ($E_{\rm res}$) by keeping the ($E_{\rm res}/T_c$) ratio [24], the enhanced pseudogap energy in the optical conductivity [25], and the decreasing incommensurability of spin-density modulations [9]. Besides, the smeared 1/8-anomaly on T_c by Ni substitution in striping LSCO [26] is attributed to the charge-dopant nature of the localized ZR doublet state, since an extra charge potential will diffuse the charge-stripe river and make the stripe order unstable. Thus, magnetic-dopant natures of Ni are commonly missing in the SC phase. Any theoretical model which regards Ni as a magnetic impurity for high-T_c superconductivity should be discarded, at least below the optimally doped regions.

In summary, we discovered two types of Ni dopant state from the raw data of polarized XAFS for $\mathbf{E}_\parallel$. Present study gives a dual picture for Ni impurity in high-T_c cuprates. That is, the Ni atom functions as a magnetic dopant of $S = 1$ (Ni^{2+}) when Ni is rich, and as a charge dopant of $Ni^{2+}\underline{L}$ ($S_{\rm eff} = 1/2$) when hole is rich. Further investigation is required to reveal the origin of the systematic changes in the intensity pattern [Fig. 1(a)] and $C_{O(1)}$ [Fig. 3(b)].

We are grateful to T. Tohyama, K. Tsutsui, W. Koshibae, and M. Kofu for their helpful discussions. We also thank M. Sakurai for growing the single crystals. This work was performed under the Common-Use Facility Program of JAEA. The work at Tohoku University was supported by the Grant-In-Aid for Scientific Research C (19540358) and B (19340090) from the MEXT.

[1] For example, *Introduction to Superconductivity*, edited by M. Tinkham (Dover Books on Physics, New York, 2004), 2nd ed.
[2] For example, *Physical Properties of High Temperature Superconductors I*, edited by D. M. Ginsberrg (World Scientific, Singapore, 1989).
[3] S. H. Pan *et al.*, Nature (London) **403**, 746 (2000).
[4] V. Bhat *et al.*, Physica C (Amsterdam) **191**, 271 (1992).
[5] P. Mendels *et al.*, Physica C (Amsterdam) **235–240**, 1595 (1994).
[6] T. Nakano *et al.*, Phys. Rev. B **58**, 5831 (1998).
[7] H. Hiraka *et al.*, J. Phys. Soc. Jpn. **74**, 2197 (2005).
[8] M. Matsuda *et al.*, Phys. Rev. B **73**, 140503(R) (2006).
[9] H. Hiraka *et al.*, J. Phys. Soc. Jpn. **76**, 074703 (2007).
[10] D. Haskel *et al.*, Phys. Rev. B **64**, 104510 (2001).
[11] We infer two types of Ni charge state: Ni^{2+} and $Ni^{2+}\underline{L}$, as explained later. For the Ni^{2+} reference of (5–100), 95% of Ni are Ni^{2+} and the remainder 5% become $Ni^{2+}\underline{L}$. Current experimental resolution cannot resolve this heavily imbalanced population.
[12] M. Kofu *et al.*, Phys. Rev. B **72**, 064502 (2005).
[13] Because of the largely imbalanced population of Ni^{2+} and $Ni^{2+}\underline{L}$ in the (1–7) sample, the assignment of both states must be difficult with current resolution.
[14] H. Hiraka *et al.*, J. Phys. Chem. Solids **69**, 3136 (2008).
[15] We need the two-shell analysis due to the short distance of ~0.9 Å between O(2) and La/Sr.
[16] For example, *X-ray Absorption: Principles, Applications, Techniques of EXAFS, SEXAFS, and XANES*, edited by D. C. Koningsberger and R. Prins (John Wiley & Sons, New York, 1988).
[17] J. R-. Carvajal *et al.*, J. Phys. Condens. Matter **3**, 3215 (1991).
[18] H. Oyanagi *et al.*, J. Phys. Soc. Jpn. **58**, 2896 (1989).
[19] P. G. Radaelli *et al.*, Phys. Rev. B **49**, 4163 (1994).
[20] A. Sahiner *et al.*, Phys. Rev. B **51**, 5879 (1995).
[21] F. C. Zhang and T. M. Rice, Phys. Rev. B **37**, 3759 (1988).
[22] G. Xiao *et al.*, Phys. Rev. B **42**, 8752 (1990).
[23] E. W. Hudson *et al.*, Nature (London) **411**, 920 (2001).
[24] Y. Sidis *et al.*, Phys. Rev. Lett. **84**, 5900 (2000).
[25] A. V. Pimenov *et al.*, Phys. Rev. Lett. **94**, 227003 (2005).
[26] Y. Koike *et al.*, Solid State Commun. **82**, 889 (1992).